RSC Advances

ROYAL SOCIETY OF CHEMISTRY

www.rsc.org/advances

Journal Name

ARTICLE

Physicochemical Characterization of Hexacyanometallate-TiO_2 Composite Materials

Received 00th January 20xx,
Accepted 00th January 20xx

DOI: 10.1039/x0xx00000x

www.rsc.org/

Mario Berrettoni,[a,b*] Michela Ciabocco,[a] Marzia Fantauzzi,[d,e] Marco Giorgetti,[b,c] Antonella Rossi[d,e] and Eugenio Caponetti[f]

The paper describes synthesis and characterization of novel TiO_2-Metal Hexacyanometallates (MHCMs) composite materials. The starting material, TiO_2, was modified by addition of cobalt-hexacyanoferrate (CoHCF) or iron-hexacyanocobaltate (FeHCC) at various concentrations. The resulting composites were charcterized as follows: cyclic voltammetry (CV) followed the formation of TiO_2-MHCM clusters, TEM micrographs studied their morphology, XAS and XPS data indicated that MHCM bonds to TiO_2 through the the nitrogen atom of its -CN group and modifies the environment of Ti compared to that of pure anatase. As expected, and confirmed by UV-Vis and XP-valence band data, the electronic properties of TiO_2 were substantially modified: the edge in the composite materials shifted by about −2.0 eV relative to TiO_2.

[a] *Dipartimento di Chimica Industriale "Toso Montanari", UOS, Campus di Rimini, Università di Bologna, Via dei Mille 39, 47921 Rimini – Italy. E-mail: mario.berrettoni@unibo.it*
[b] *INSTM, UdR Bologna – Italy.*
[c] *Dipartimento di Chimica Industriale "Toso Montanari", Università di Bologna – Italy.*
[d] *Dipartimento di Scienze Chimiche e Geologiche, Università degli Studi di Cagliari, Campus di Monserrato S.S. 554 – Italy and INSTM, UdR Cagliari – Italy.*
[e] *Centro Grandi Strumenti Università degli Studi di Cagliari – Campus di Monserrato S.S. 554 – Italy.*
[f] *Dipartimento STEBICEF Università degli studi di Palermo – Italy.*
Electronic Supplementary Information (ESI) available. See
DOI: 10.1039/x0xx00000x

Journal Name

ARTICLE

Introduction

Composite materials consisting of semiconductors and inorganic compounds have often attractive photo-electrochemical properties. Among the semiconductor materials, TiO_2 is particularly promising due to its photo-electrochemical properties, high photo-activity, outstanding hydrophilicity[1], strong redox and catalytic activity; the range of its potential applications includes catalysis, photovoltaic cells, self-cleaning and antifogging surface treatments[2,3,4,5,6,7.] In addition, TiO_2 is non-toxic, chemically very stable, and easily obtained as nanometer scale particles[8].

The photo-catalytic properties of TiO_2 are strongly affected by its structure, interface, grain size and crystallographic orientation of the exposed faces in contact with solution.[9] The photo-electrochemical characteristics are dependent upon porosity, morphology and the method of synthesis[10,11]. Surface functionalization of TiO_2 has been achieved with many methods including doping with metal ions or nonmetallic elements, sensitization with organic dyes or semiconductors with a small band-gap.

The aim of this paper is the design, synthesis and characterization of new composite materials of TiO_2 and metal hexacyanometallates.

Metal-hexacyanometallates (MHCMs) are solid compounds of mixed valence with general formula: $A_xM_y[B(CN)_6]\cdot nH_2O$ where M and B are transition metals, A an alkaline metal, x and y stoichiometric coefficients, n the hydration-intercalation molecules per unit formula (≤ 14). Metal hexacyanoferrates (MHCFs) are a class of mixed-valence compounds of major technological interest for their electrocatalytic,[12] electrochromic,[13,14] ion-sensing,[15] ion-exchanging[16] and photomagnetic[17] properties and also for their possible applications in batteries and charge-storage devices[18]. These salts present a face centered cubic (fcc) unit cell and depending upon the degree of peptization, can be described in the "soluble" and the "insoluble" form. Basically, the insoluble form lacks one-fourth of the $B(CN)_6^{3-}$ units, which are replaced by coordinated and non-coordinated water molecules[19].

Among the hexacyanoferrates, cobalt hexacyanoferrate (CoHCF) has been extensively studied in literature due to its interesting chemical and electrochemical properties[20] and its ease of synthesis by chemical and electrochemical deposition.

Iron hexacyanocobaltate, FeHCC presents a cubic structure similar to that of CoHCF, but with metal centers differently coordinated to either carbon or nitrogen and with significantly different properties. The electrochemistry of FeHCC has not been as extensively investigated as that of CoHCF. However, in FeHCC only iron centers are electroactive while Co atoms in aqueous electrolytes display no activity[21].

Widmann et al. studied the solid mixtures $KM[hcf]_{1-x}[hcc]_x$ where M = Ni, Fe, Cu, and demonstrated the redox activity of high spin iron centre Fe^{2+}/Fe^{3+}. This activity is observed by cyclic voltammetry only in freshly synthesized FeHCC; after 2 days the features of low-spin iron appear, obviously due to a partial decomposition to Prussian green revealed by a change in color to light green[22].

TiO_2 nanoparticles functionalized with $Fe^{II}(CN)_6^{4-}$ have been investigated by electro-absorption spectroscopy. The iron complex is believed to bind at a surface Ti^{IV}-site via a mono-dentate cyanide ligand, $(CN)_5Fe^{II}$-CN-Ti^{IV}(particle)[23], as suggested by IR and resonance Raman evidence. Other studies dealt with thin films prepared by mixing TiO_2 with metal-hexacyanometallates.[24,25,26,27] To the best of our knowledge, no investigation of the CoHCF–TiO_2 composites has been reported while a detailed study of their FeHCC–TiO_2 counterparts has appeared[27].

An aim of this paper is to compare the photo-electrochromic and photo-electrochemical behavior of CoHCF–TiO_2 composites with that of their FeHCC–TiO_2 counterparts. Here, we will also detail the procedure of synthesis, and their influence upon optical properties, and the structural-electronic characterization performed with a wide range of experimental techniques.

Experimental

Chemicals and Solutions

All chemicals used in this work were reagent grade and were used as received from Sigma-Aldrich ($FeCl_2$, $K_3[Co(CN)_6]$, $K_3[Fe(CN)_6]$, $CoCl_2$, KCl, anatase TiO_2 99%) and from Fluka ($TiCl_4$, >99.0%). Deionized water was used throughout this work. All experiments were carried out at room temperature and in air.

Electrochemical Measurement

Electrochemical measurements were carried out with a CH Instrument, model 660c, through a standard three-electrode electrochemical glass cell (10 cm^3) comprising a glassy carbon electrode (with a 3 mm diameter) as working electrode and a Pt auxiliary electrode; the reference was a silver–silver chloride electrode (Ag/AgCl) in a saturated solution of potassium chloride. All the potentials will be referred to the Ag/AgCl electrode.

An aqueous suspension of the sample was dropped on the glassy carbon electrode; after drying, an adherent deposit was

covering the electrode surface. Before deposition, the glassy carbon surface was polished with a 0.05 µm alumina slurry on a microcloth polishing pad and rinsed with deionized water.

Chemical Synthesis

Iron hexacyanocobaltate and cobalt hexacyanoferrate were synthesized by precipitation mixing 0.05 M water solution of $FeCl_2$ or $CoCl_2$ drop wise to an equivalent amount of $K_3[Co(CN)_6]$ or $K_3[Fe(CN)_6]$ and stirring at room temperature.
All precipitates were allowed to stand for a night and air-dried at ambient conditions to improve the formation of the TiO_2-MHCM bond. Subsequently, they were carefully washed with deionized water to remove the unreacted salts and centrifuged to separate the solid product. Finally, the precipitate was dried at 80°C.
TiO_2-FeHCC and TiO_2-CoHCF were obtained in a similar way starting with a TiO_2 suspension to which a water solution of $FeCl_2$ or $CoCl_2$ and an equivalent amount of $K_3[Co(CN)_6]$ or $K_3[Fe(CN)_6]$ were added drop wise and stirred at room temperature[27]. These TiO_2-MHCM compounds were synthetized in three different molar ratios: 1:1:1, 10:1:1 and 100:1:1 (where the notation indicates the TiO_2:$K_3Fe(CN)_6$:$CoCl_2$ in the case of TiO_2-CoHCF composite). The selected ratios were chosen in order to avoid the formation of a solid solution between TiO_2 and MHCMs. Hereafter, the composites will be identified by the notation 1:1, 10:1, 100:1.

X-ray Diffraction (XRD)

XRD measurements were performed on a Rigaku Mo Kα X-ray source equipped with a Huber goniometer. Cell parameter, *a*, referred to the cubic structure, was calculated by the unit cell program[28].

Transmission Electron Microscopy (TEM) and Energy Dispersive Spectroscopy (EDS)

Each dispersion resulting by mixing the powder with isopropanol was deposited on a 300-mesh nickel grid, "holey carbon-coated". TEM experiments were performed on a high-resolution transmission electron microscope (HR-TEM) JEOL JEM-2100 operating at 200 kV. Elemental analysis was carried out using an energy dispersive X-ray detector (EDS), Oxford mod. 6498, with a 30 mm^2 area.

Fourier Transform Infrared Spectroscopy (FT/IR)

Infrared spectra (IR) were recorded with a Jasco FT/IR-4600 PLUS spectrometer working in transmission mode. At least 32 scans were typically taken between 4000 cm^{-1} and 500 cm^{-1} with a resolution of 1 cm^{-1}. Powder spectra were recorded by using KBr pellets, containing about 1% w/w of the sample. The pellets were produced by compressing with 5 ton for about 20 s the powders in a stainless steel mold of 13 mm in diameter; no pressure effects have been observed by using a manually operated hydraulic press (Specac Ltd., Orpington Kent, UK). The spectrum of pure KBr was taken as a background reference.

X-ray photoelectron spectroscopy (XPS)

X-ray photoelectron spectroscopy (XPS) analyses were performed with a Thetaprobe spectrometer (Thermo Fisher Scientific, Waltham MA, USA) at the University of Cagliari. The samples were mounted as pellets on a copper bi-adhesive tape. Spectra were collected using a 300 µm spot size Al Kα monochromatic beam operated at 4.7 mA and 15 kV. A flood gun was used for charge compensation. Survey spectra were acquired in fixed analyzer transmission mode (FAT) using a pass energy (PE) of 200 eV, while the high-resolution spectra of C1s, Cl2p, Co2p, Fe2p, K2p, N1s, O1s, Ti2p were collected with a PE of 100 eV selecting the standard lens mode; the full-width at half-maximum of the peak height, FWHM, of the silver $Ag3d_{5/2}$ signal for the high-resolution spectra was 0.83 eV. The linear response of the instrument was checked with periodic calibrations performed according to ISO 15472:2001[29].
Binding energy values were corrected by referencing the aliphatic carbon to 285 eV. Data were acquired under computer control (Avantage v 3.45). The spectra were processed using CASAXPS software.[30] An iterated Shirley – Sherwood[31] background subtraction routine was performed before applying a fitting procedure using a combination of Gaussian and Lorentzian shapes. Composition was calculated using the first-principle method[32] and assuming a homogeneous sample. Peak areas were corrected for the sensitivity factors calculated using the Scofield's photoionization cross-sections[33], the asymmetry parameters[34], the inelastic mean free paths (IMFP) and the intensity/energy response of the analyzer as detailed in the literature[35]. IMFP were calculated according to Seah et al.[36] The accuracy of the resulting atomic concentrations is estimated to be within ± 10%.

UV-Visible Spectroscopy

UV-Vis spectra were recorded in the 220–700 nm range with a HEλIOS α THERMO SPECTRONIC instrument.

Thermogravimetric Analysis (TGA)

Thermogravimetric analyses (TGA) were carried out in a Perkin Elmer TGA7 thermogravimetric analyzer. Samples (between 5 and 10 mg) were heated from 25 to 400°C at 5°C/min under flowing nitrogen (20 cm^3/min).

X-ray Absorption Spectroscopy (XAS)

X-Ray absorption measurements have been recorded at the XAFS beamline at Elettra Synchrotron (Basovizza, Trieste, Italy). The storage ring operated at 2.0 GeV in top up mode with a typical current of 300 mA. The data were recorded at Ti K-edge (4965 eV), Fe K-edge (7112 eV) and Co K-edge (7709 eV) in transmission mode using ionization chamber. Samples for XAS measurements were solid pellets, prepared by mixing the material (15 mg) with cellulose filler (100 mg). XAS spectra were deglitched, calibrated, and normalized using the Athena program[37].

Results

Table 1 lists the TiO_2-FeHCC and TiO_2-CoHCF composite materials synthetized in different ratios and summarizes the techniques used for their characterization. The results of the thermogravimetric analyses and the XRD are also included. TGA allows the determination of the number of water molecules included in the structure of the hexacyanometallate. In Table 1 the XRD column reports the cell parameter, *a*, referred to the cubic structure, calculated by the unit cell program.

The diffractogram of the 100:1 TiO_2:FeHCC sample is not available being the concentration of FeHCC too low in this composite. The cell parameters, *a*, assume a value very close to 10 Å, typical of the hexacyanometallates.

Table 2 provides the stoichiometry of the compounds as measured by X-ray fluorescence (XRF) and X-ray photoelectron spectroscopy (XPS). K^+ is missing in the XRF data due to limitations of the experimental set up.

The low intensity of the cobalt signal, Co2p, did not allow calculation of the surface composition of the TiO_2-FeHCC sample in 100:1 ratio. The elemental ratios calculated with XPS and XRF are in reasonable agreement.

Table 1 Summary of the compounds studied.

Sample		CV	IR	UV-Vis	TGA (nH_2O)*	XAS	XRD a / Å*	XPS	TEM
TiO_2-CoHCF	1:1	X	X	X	3,0	X	10.07	x	X
	10:1	X	X	X	6,5		10.30	x	X
	100:1	X	X	X	7,8		10.26	x	X
TiO_2-FeHCC	1:1	X	X	X	5,2	X	10.30	x	X
	10:1	X	X	X	6.3		10.13	x	X
	100:1	X	X	X	7.4		-	x	X

*The last digit is only partially significant due to the statistical error.

Table 2 Stoichiometry of the studied compounds, obtained by XPS and XRF techniques.

Sample	TiO_2:MHCM Ratio	XPS			XRF*	
		Formula	**Co/Fe**	**N/Fe**		**Co/Fe**
TiO_2 + CoHCF	1:1	$K_{1.2}Co_{1.3}[Fe(CN)_6]$	1.3	6.5	$Co_{1.1}[Fe(CN)_6]$	1.1
	10:1	$K_1Co_{1.5}[Fe(CN)_6]$	1.5	6.3	$Co_{1.2}[Fe(CN)_6$	1.2
	100:1	$K_{0.7}Co_{1.5}[Fe(CN)_6]$	1.5	5.9	$Co_{1.4}[Fe(CN)_6]$	1.4
			Fe/Co	**N/Co**		**Fe/Co**
TiO_2 + FeHCC	1:1	$K_{0.7}Fe_{0.7}[Co(CN)_6]$	0.7	6.2	$Fe_{0.8}[Co(CN)_6]$	0.8
	10:1	$K_{0.3}Fe_{0.8}[Co(CN)_6]$	0.8	5.8	$Fe_{1.6}[Co(CN)_6]$	1.6
	100:1	-	-	-	$Fe_{1.32}[Co(CN)_6]$	1.3

*K^+ is not detected.

All the compounds prepared, TiO_2-FeHCC and TiO_2-CoHCF in different ratios, were fully characterized by CV, TEM, IR, UV-Vis, XAS and XPS in order to provide evidence of their formation, to determine the morphology of the aggregates, to verify the formation of the compounds and to shed a light on the effect of the FeHCC and CoHCF doping agents.

Journal Name

ARTICLE

Cyclic voltammetry (CV)

TiO_2-FeHCC and TiO_2-CoHCF compounds were synthetized, deposited on glassy carbon and characterized by cyclic voltammetry. Fig. 1 shows the voltammograms for TiO_2-FeHCC (black line) and TiO_2-CoHCF (red line), both in a 1:1 TiO_2-MHCM ratio.

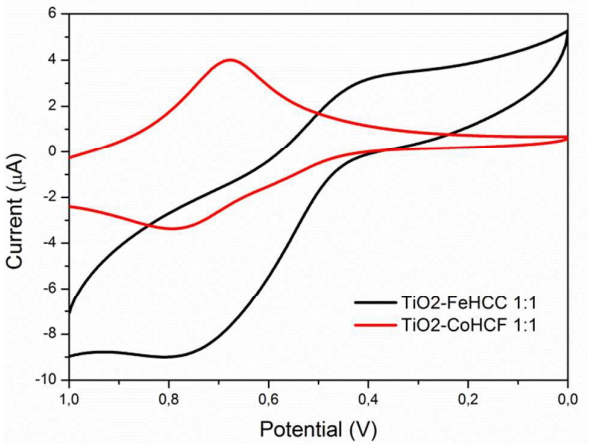

Fig. 1 CVs at 0.1 V/s of TiO_2-FeHCC 1:1 (black line) and TiO_2-CoHCF 1:1 (red line) in a 1.0 M KCl solution. Potentials are referred to the saturated Ag/AgCl electrode.

Fig. 2 and 3 provide CVs of TiO_2-FeHCC and TiO_2-CoHCF in 1:1, 1:10, 1:100 molar ratios respectively, in 1.0 M KCl solution. In all cases, only a single reversible redox system is observed.

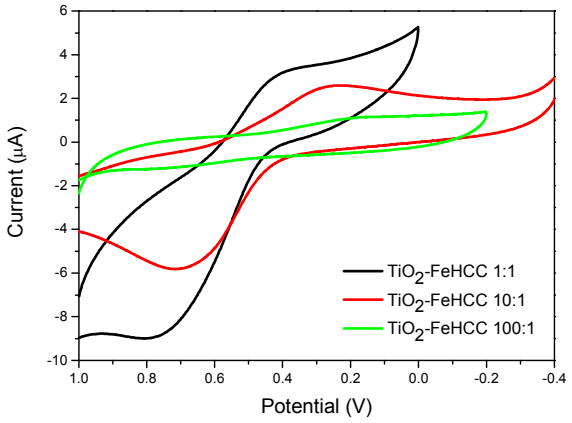

Fig. 2 CVs at 0.1 V/s of TiO_2-FeHCC 1:1 (black line), 10:1 (red line), 100:1 (green line) in a 1.0 M KCl solution. Potentials are referred to the saturated Ag/AgCl electrode.

Table 3 and 4 report the Ep_c and Ep_a (in Volts) values for the 1:1, 10:1 and 100:1 TiO_2-FeHCC and TiO_2-CoHCF compounds respectively and the relative E^0 values calculated as $(Ep_a+Ep_c)/2$.

Table 3 Ep_c and Ep_a (in Volts) for the 1:1, 10:1 and 100:1 TiO_2-FeHCC compounds and the relative E^0 value.

TiO_2-FeHCC	Ep_c	Ep_a	E^0
1:1	0.364	0.787	0.575
10:1	0.261	0.708	0.484
100:1	0.207	0.735	0.471

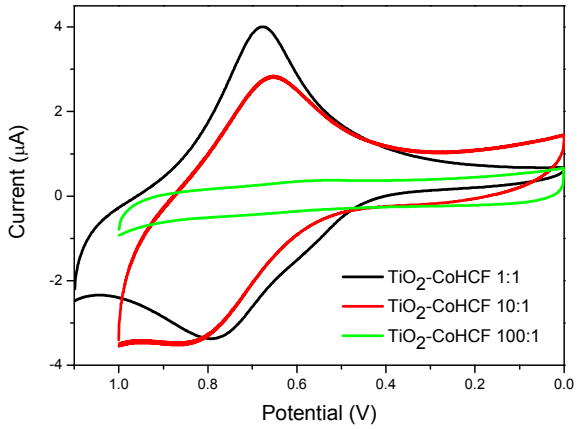

Fig. 3 CVs at 0.1 V/s of TiO_2-CoHCF 1:1 (black line), 10:1 (red line), 100:1 (green line) in a 1.0 M KCl solution. Potentials are referred to the saturated Ag/AgCl electrode.

Table 4 Ep_c and Ep_a (in Volts) for the 1:1, 10:1 and 100:1 TiO_2-CoHCF compounds and the relative E^0 value.

TiO_2-CoHCF	Ep_c	Ep_a	E^0
1:1	0.679	0.784	0.732
10:1	0.655	0.835	0.745
100:1	0.529	--	--

CVs were also performed in solution with different KCl concentrations (1.0, 1.0×10^{-1}, 1.0×10^{-2} M) to verify the role of K^+. For both compounds, the peak potentials shifted in the negative direction with decreasing the electrolyte concentration, thus confirming that the redox process is associated with the intercalation of electrolyte K^+ cations (see Fig. S1 and S2 in the supporting information). Within the experimental error, the slopes of 56 mV and 52 mV are consistent with a single electron redox process assisted by K^+.

Similar results were obtained for TiO_2-FeHCC and TiO_2-CoHCF in 10:1 molar ratio (not shown).

Transmission Electron Microscopy (TEM)

All samples were characterized by transmission electron microscopy (TEM) and energy dispersive spectroscopy (EDS) to provide evidence for the presence of the metal hexacyanometallate and to characterize the morphology of particles and aggregates. In particular EDS analyses performed upon various aggregates confirm the co-presence of Fe, Co, and Ti. The following observations apply to FeHCC and CoHCF compounds:

aggregates of TiO_2-CoHCF (1:1 ratio) and TiO_2-FeHCC (1:1 ratio) consist of typical spherical TiO_2 particles covered with grains of cubic CoHCF and FeHCC (see Fig. S3 a,b);

in 1:1 samples, many isolated clusters of CoHCF or FeHCC with cubic structure and 100 ÷200 nm in size are observed; however, FeHCC has less isolated clusters than CoHCF.

in 10:1 samples; TiO_2 aggregates are larger, ranging from 100 to 600 nm, and consist of 5÷20 TiO_2 spherical particles; Fig. 4 is a micrograph of TiO_2 and CoHCF in 10:1 ratio showing an aggregate of spherical TiO_2 particles covered with cubic nanocrystals of CoHCF.

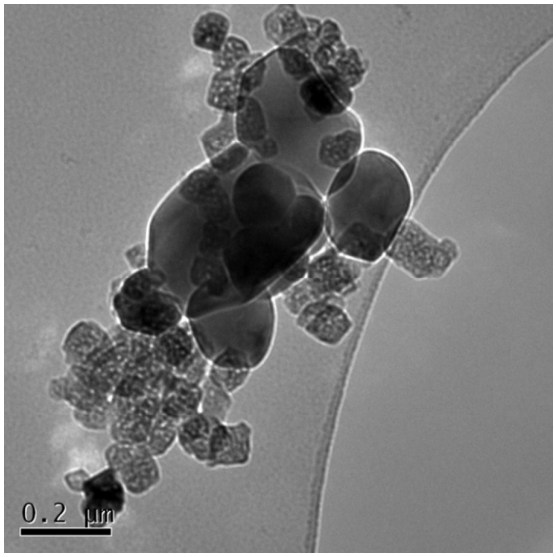

Fig. 4 Typical aggregate of TiO_2 spherical particles covered with cubic nanocrystals of CoHCF (10:1 ratio).

In 100:1 samples, rare CoHCF or FeHCC grains and TiO_2-CoHCF or TiO_2-FeHCC aggregates are present, as shown in Fig. 5. These CoHCF or FeHCC grains are larger than in the 1:1 and 10:1 samples.

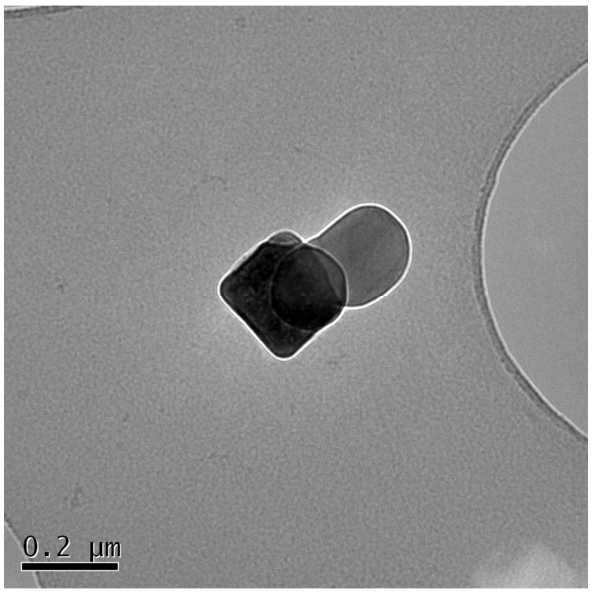

Fig. 5 Magnification at 30.000x of the sample referring to a cubic particle of CoHCF bonded to a TiO_2 spherical particle. TiO_2-CoHCF are in 100:1 ratio.

Fourier transform Infrared Spectroscopy (FT/IR)

For sake of clarity and comparison, each Fourier transform infrared (FT/IR) spectrum presented below is overturned and individually normalized to its top transmittance value. Fig. 6 shows the spectra of FeHCC (red curve) and CoHCF (black curve) in the bulk form. The CN stretching bands are eventually decomposed by curve fitting in order to assign the main bands. The spectra of Fig. 6 agree with data from the literature[20,27].

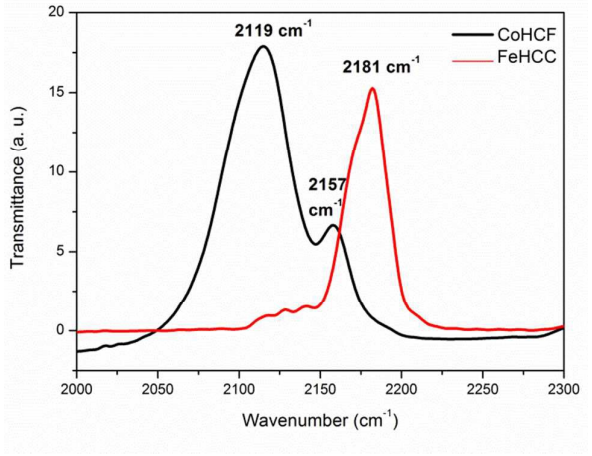

Fig. 6 FeHCC (red curve) and CoHCF (black curve) FT/IR spectra in the 2000-2300 cm^{-1} range.

Fig. 7 and 8 show the normalized IR transmission spectra in the region of the CN stretching frequencies for TiO_2-CoHCF and TiO_2-FeHCC, respectively, in different molar ratios (1:1, 10:1 and 100:1).

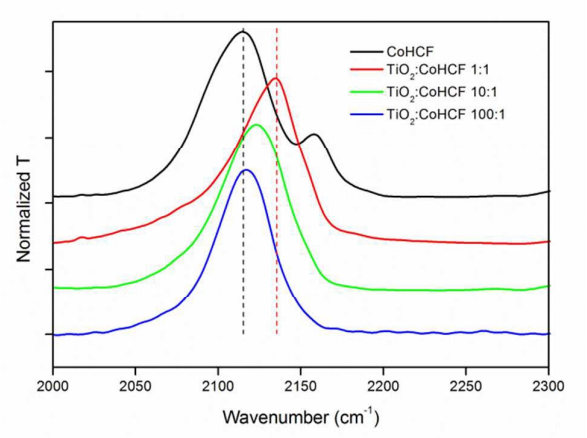

Fig. 7 TiO_2-CoHCF FT/IR spectra at different molar ratios in the region of CN stretching frequencies.

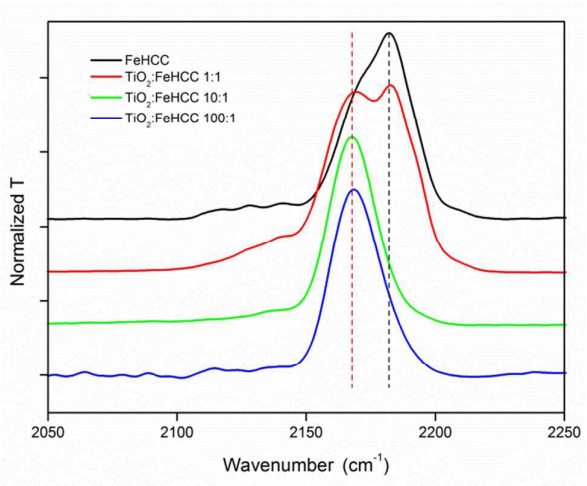

Fig. 8 TiO_2-FeHCC FT/IR spectra in different molar ratios in the in the region of CN stretching frequencies.

Table 5 CN stretching frequencies in CoHCF and TiO_2-CoHCF from curve-fitting.

Stretching	Fe^{II}-CN-Co^{II} ῡ / %	Fe^{II}-CN-Co^{III} ῡ / %	Fe^{II}-CN-Co^{III} ῡ / %	$Fe^{II/III}$-CN-Ti ῡ / %	Fe^{III}-CN-Co^{II} ῡ / %
Bulk	2081 / 11	2102 / 36	2119 / 33	2133 / 0	2157 / 20
1:1	2081 / 20	2102 / 16	2119 / 28	2133 / 35	2157 / 1
10:1	2081 / 15	2102 / 17	2119 / 37	2133 / 31	2157 / 0
100:1	2081 / 20	2102 / 8	2119 / 66	2133 / 0	2157 / 6

In the bulk CoHCF compound, we detected and assigned all the bands due to the possible combinations $Fe^{II/III}$-CN-$Co^{II/III}$ (see Table 5). In the 1:1 and 10:1, the bands at 2157 cm^{-1} disappear, the bands at 2081, 2102 and 2119 cm^{-1} remain nearly the same, a new band at 2133 cm^{-1} appears, probably due a $Fe^{II/III}$-CN-Ti bond. In the 100:1 compound the band distribution density is similar to the bulk one. These findings fully agree with the XPS results (see the XPS section) and are consistent with the pictures emerging from the TEM analyses. In fact, in the 100:1 compound, the CoHCF particles bonded to TiO_2 are very few while clusters of isolated CoHCF are mostly detected.

Table 6 reports the same data for the observed CN stretching bands in FeHCC, without any assignment to a definite chemical structure, the bands are indicated only as ῡ 1, ῡ 2 and ῡ 3 because no reference data have been found in literature. Anyway, the whole IR band is in agreement with Berrettoni et al[27]. The difference in the relative intensity of the bands, especially relevant in the case of FeHCC, can be due to different particle size (i. e. the bulk surface features) and it will not be discussed here.

Table 6 CN stretching related to different chemical features of FeHCC. ῡ 1, ῡ 2 and ῡ 3 indicate the observed bands. Peak areas in percentage are also provided.

Stretching	ῡ 1 / %	ῡ 2 / %	ῡ 3 / %
Bulk	2167 / 21	2169 / 0	2181 / 79
1:1	2167 / 28	2169 / 38	2181 / 34
10:1	2167 / 26	2169 / 74	2181 / 0
100:1	2167 / 28	2169 / 44	2181 / 27

In the bulk compound, two stretching bands are observed at 2181 and 2167 cm^{-1}. The intensity of the band at 2181 cm^{-1}, the dominant one in bulk FeHCC, decreases by dilution with TiO_2 while the intensity of the band at 2169 cm^{-1} , absent in bulk FeHCC, increases; the latter band is tentatively assigned to the FeHCC-TiO_2 bond. The intensity of the band at 2167 cm^{-1} is not influenced by the concentration, as shown in Table 6, so it can be referred to the FeHCC in bulk. In the case of FeHCC we observe a net shift between CN in the bulk form and CN in the TiO_2-linked form. Furthermore, the shift is inversely proportional to the FeHCC concentration. The spectra of the samples with CoHCF have more features than those with FeHCC, corresponding to a relatively minor complexity of the latter.

X-ray photoelectron spectroscopy (XPS)

X-ray photoelectron spectra were acquired with the full set of compounds. Survey spectra of TiO_2-CoHCF in 1:1, 10:1 and 100:1 ratios are shown in Fig. S4 of the supporting information. Signals from all the elements that belong to the compounds C, N, O, Fe, Co, Ti, K and a small amount of Cl have been detected. These elements are revealed on the surfaces of TiO_2-FeHCC aggregates at all dilutions (see Fig. S5 in the supporting information). The quantitative analyses are summarized in Table 2; we have a fairly good agreement with the energy dispersive spectroscopy data, compatible with the experimental uncertainties of the two techniques.

To obtain information about the chemical state of the elements, the spectra of iron, cobalt, nitrogen and titanium were curve fitted. Parameters such as the Gaussian-Lorentzian ratio and the full width at half height (FWHH) of a component were obtained from the spectra of reference compounds taken under identical acquisition conditions[55,56].

Iron

Fig. 9a shows, as examples, the fitting of the $Fe2p_{3/2}$ signals in the 1:1 TiO_2–CoHCF and TiO_2–FeHCC samples. The $Fe2p_{3/2}$ peak of the bulk CoHCF indicates the presence of Fe^{II} (B.E. = 708.4 eV) and Fe^{III} (B.E. = 710.0 eV), in agreement with

literature[38,39] (see Fig. S6 in the supporting information); this agrees with the IR spectra of CoHCF in the bulk form (Fig. 7 and Table 5). The absence of Fe^{III} in TiO_2-CoHCF samples with 1:1 (Fig. 9a) and 10:1 ratios (Supporting information Fig. S8) confirms the IR results. The presence of a component at 710 eV in the 100:1 sample (see Fig. S6 in the supporting information), associated with the presence of Fe^{III}, is also in agreement with the IR findings.

The line shape of $Fe2p_{3/2}$ in the FeHCC compounds is very different from that in CoHCF (Figure 9a and Fig. S7 in the supporting information): the peaks are asymmetric, the full-width at half height (FWHH) is greater, and peak positions are shifted to higher binding energies. Curve fitting procedures performed according to literature[40,41] lead to the conclusion that both Fe^{II} at 709.0 eV and Fe^{III} at 710.5 eV are present at the surface of FeHCC grains.

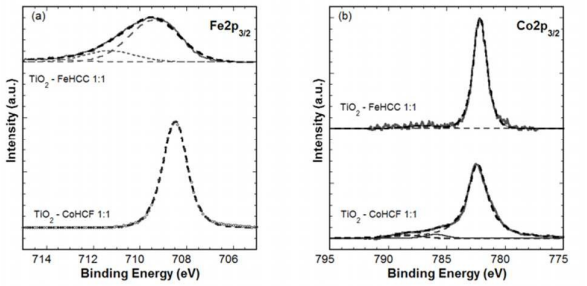

Fig. 9 XPS $Fe2p_{3/2}$ (a) and $Co2p_{3/2}$ (b) spectra of 1:1 TiO_2–CoHCF and TiO_2–FeHCC samples.

Cobalt

In Fig. 9b curve fitted $Co2p_{3/2}$ signals of 1:1 TiO_2–CoHCF and TiO_2–FeHCC samples are reported as examples. In the CoHCF compounds, the $Co2p_{3/2}$ feature has a main component at 782.0 ± 0.2 eV together with shake-up satellites peaks at higher binding energies. These satellites suggest the existence of Co(II)[42,43,44]. No significant chemical shift is observed for Co^{II} and Co^{III}–CN complexes[45] but the co-presence of Co^{III}, which was revealed by IR spectroscopy, is supported by the difference in binding energy, $\Delta E = Co2p_{1/2} - Co2p_{3/2}$, which is about 15.6 eV, intermediate between the value reported for Co^{II} (16 eV) and the one for Co^{III} (15 eV). The absence of satellites in the $Co2p_{3/2}$ feature of the FeHCC compounds (Fig. 9b) and a binding energy separation $Co2p_{1/2} - Co2p_{3/2}$ of 15 eV strongly implies that cobalt is present as Co^{III} in these compounds.

Nitrogen

N1s signal for CoHCF and FeHCC samples without TiO_2 shows a single component at 398.3 ± 0.2 eV; in the presence of TiO_2, a second small component appears at a higher binding energy (399.5 ± 0.2 eV) (Fig. 10a,b). The most intense signal could be ascribed to nitrogen of the cyano-groups coordinating a transition metal[46]. The weaker signal might be assigned to the M–CN–Ti surface complexes, as described by Macyka et al[47]. The intensity of the second component increases from TiO_2–MHCM 1:1 to TiO_2–MHCM 100:1 (Fig. 10c) and the increase of the intensity is more pronounced in the case of TiO_2-CoHCF than for TiO_2-FeHCC samples. The detailed N1s spectra of all the samples studied in this paper are provided in Fig. S8 and S9 of the supporting information.

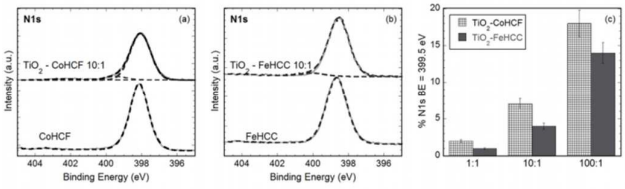

Fig. 10 N1s signal from CoHCF (a) and FeHCC (b) compounds. c) area % of the second component of N1s (B.E. = 399.5 eV) for all the TiO_2-MHCM compounds.

Titanium

Ti2p peaks (Fig. S10 in the supporting information) were curve fitted, after Shirley-Sherwood background subtraction, with a doublet (Ti2p1/2 – Ti2p3/2) separated by 5.7 eV due to spin-orbit coupling. Each peak is symmetric; the binding energy of Ti2p3/2 peak is found at 458.8 eV in the 1:1 samples, as for TiO_2, and shifts to 459.2 eV in the 100:1 samples. The effective invariance of the above parameters could be due to the fact that the Ti2p signal is mainly due to the unbounded TiO_2 particles.

Table 7 Ti2p binding energy value for hexacyanometallate-TiO_2 composites.

$Ti2p_{3/2}$ binding energy value (eV ± 0.2)		
TiO_2:MHCM	FeHCC	CoHCF
1:1	458.9	458.8
10:1	458.8	458.8
100:1	459.2	459.1

XP-Valence Band

XP-valence bands of TiO_2 and TiO_2–MHCM compounds have been recorded and results are shown hereafter (Fig. 11 and 12). Pure TiO_2 valence band edge shows the presence of two peaks, separated by ~2 eV that could be ascribed to π (nonbonding) and σ (bonding) O2p orbitals[48].

CoHCF compounds

Fig. 11 shows the valence bands of cobalt hexacyanoferrate without TiO_2 and in the mixtures 1:1 and 1:10 with TiO_2 . The valence band of commercial TiO_2 (Sigma Aldrich) is provided for comparison. The band is due to the overlapping of the contributions due to Co-N σ and π bonding electrons, with Fe-C σ and π bonding and Co non – bonding electrons[49]. Relative to pure TiO_2 , the edge shifts to lower binding energies in bulk CoHCF and its mixtures with TiO_2 (Table 8).

Table 8 Comparison of the valence band edge binding energy of CoHCF and TiO_2-CoHCF compounds at different ratios.

Sample	Valence Band Edge binding energy (eV ± 0.2)
CoHCF	2.0
TiO_2:CoHCF 1:1	1.2
TiO_2:CoHCF 10:1	1.2
TiO_2	3.2

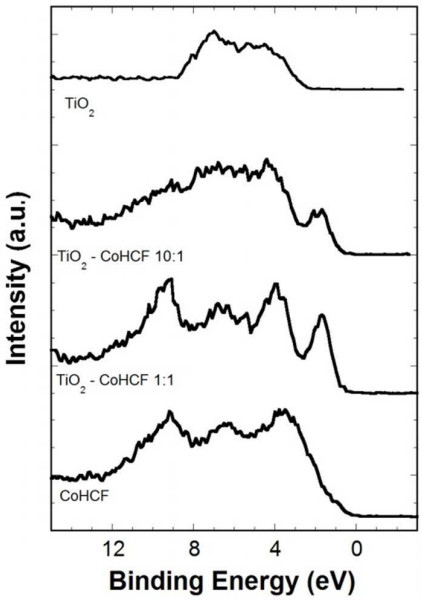

Fig. 11 XPS valence bands of CoHCF compounds and of commercial titania (0-15 eV region).

FeHCC compounds

Fig. 12 shows the valence bands of the iron hexacyanocobaltate compounds.

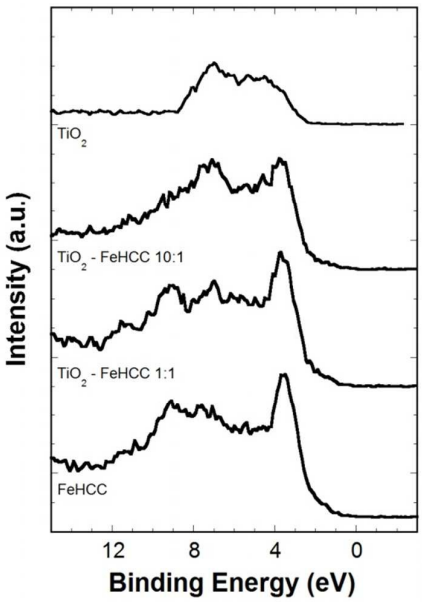

Fig. 12 XPS valence bands of FeHCC compounds and of commercial titania (0-15 eV region).

Also in this case a complex band between 0 and 12 eV is observed for pure FeHCC; in analogy with CoHCF, it is assigned to the overlapping of the bands due to Co-C σ and π bonding electrons with Fe-C σ and π bonding electrons. A shift toward lower energies of the edge is also observed (Table 9) in the TiO_2–MHCM composites relative to pure TiO_2; a difference of 0.7 eV is observed between the edge of bulk CoHCF and that of bulk FeHCC.

Table 9 Comparison of the valence band edge binding energy of FeHCC and TiO_2-FeHCC compounds at different ratios.

Sample	Valence Band Edge binding energy (eV ± 0.2)
FeHCC	1.3
TiO_2:FeHCC 1:1	1.3
TiO_2:FeHCC 10:1	1.9
TiO_2	3.2

X-ray absorbance spectroscopy (XAS)

Relevant information on about the binding between TiO_2 and the hexacyanometallates can be gained by using an elemental analytical technique such as the X-ray Absorption Spectroscopy[50]. In this case, all the three metal sites (Ti, Fe, Co) can be monitored and the results are shown in Fig. 13.

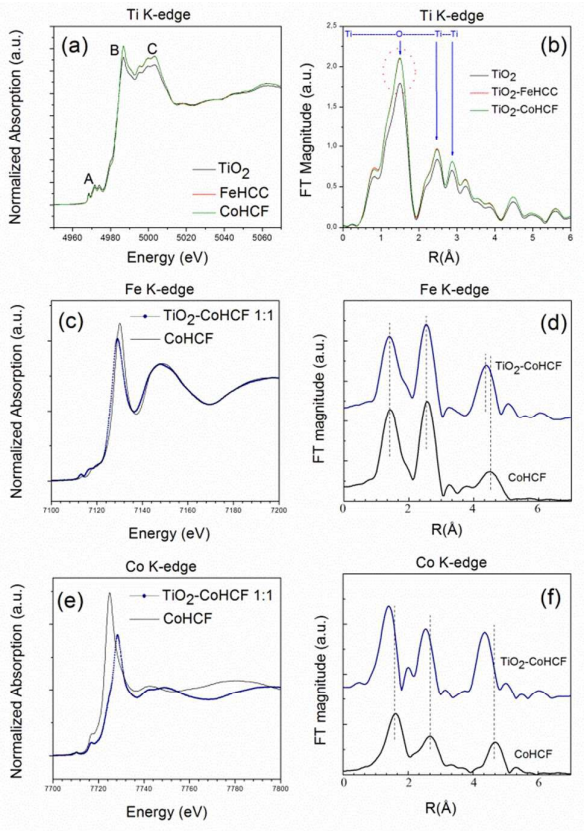

Fig. 13 XAS results of the metal sites Ti, Fe, Co. Figs (a), (c) and (e) are the normalized X-Ray Absorption Near Edge (XANES) spectra while (b), (d) and (f) are the Fourier Transforms (FTs) of the Extended X-Ray Absorption Fine Structure (EXAFS) spectra.

The normalized XANES spectra are given in the left column of Fig. 13, (a, c, e) whereas the right column provides the Fourier Transforms (FTs) of the Extended X-Ray Absorption Fine Structure (EXAFS) spectra. Of the composite samples, we report only the spectra of TiO_2–MHCM 1:1, taken as the most representative. The normalized curves at the Ti K-edge (panel (a)) give evidence that the presence of FeHCC or CoHCF modifies the local environment of titanium, in comparison with that of pure anatase phase. This is evident from the pre-edge structures (A peak), the main absorption edge (B) and the resonance (C) but the modification at the Ti site with either FeHCC or CoHCF dopant is essentially the same. The comparison of the Fourier Transform curves of the EXAFS signals relatives to the K-edge of Ti confirms minor but significant modifications of the local structure of Ti. This is showed in the panel (b) where the FTs, which are related to the radial atomic distribution around the selected (photo-absorber) atom, display peaks intensity increasing following FeHCC or CoHCF doping. This might be due to a decreasing of the structural order in the three shells as indicated in Fig. 13b.

By tuning the x-ray beam to a precise metal edge, complementary information is available at the Fe and Co K-edges for both TiO_2-FeHCF 1:1 and TiO_2-CoHCF 1:1 samples.

Panels (c), (d), (e), (f) display a selection of the XAS analysis concerning the CoHCF composites; comparison with bulk CoHCF is also provided. All panels indicate modification relative to the bulk sample of the XAS spectra, thus confirming the occurrence of a substantial interaction between TiO_2 and CoHCF.

A close inspection of the figures reveals the following details of the TiO_2-CoHCF binding. (1) the Fe local site is basically the same upon TiO_2 addition as seen from the XANES in the panel c but a shift towards lower energy of the curve is evidenced, indicating a partial reduction to Fe(II). (2) unlike the Fe, the Co local environment changes upon TiO_2 addition, as the overall shape of the XANES curve of panel (e) is strongly modified; furthermore, no changes in the pre-edge peak position has been detected and therefore the Co is in the Co(II) site.

The trend observed in the XANES data is confirmed by the corresponding FTs curves. The Fe display (panel (d)) similar peak positions and intensities, with the exception of the 3rd peak at ~5 Å, assigned to the Fe–Co distance, which decreases upon doping with TiO_2. On the contrary, all three peaks displayed in the panel (f) shift to lower distances, providing evidence for shorter bond lengths of the first, second and third shells around cobalt.

Similar comments apply to the comparison of the Fe and Co K-edges in FeHCC and TiO_2-FeHCC. The analysis, available in the supporting information, leads to the same conclusions if we swap the Co with Fe site. In this case the Fe site changes significantly upon TiO_2 doping while the Co one does not, as clearly visible from the XANES curve of Fig. S11, panels (c),(d). This experimental finding is interesting and can be explained by considering the local probe characteristic of a XAS experiment. Regardless the long range structure, the XAS indicates that significant changes occur only at the metal site (either Co or Fe), which is linked to the N side of the CN moieties of the cyanide bridge.

Discussion

Experimental evidence of the formation of composites

First of all, our findings prove how feasible and reliable is the synthesis of composite materials based on TiO_2 particles modified by CoHCF or FeHCC. In fact, electrochemical results and TEM micrographs give evidence of the formation of MHCM clusters on the TiO_2 surface. The optimum TiO_2–MHCM ratio is found between 1:1 and 10:1 since in these molar ratios the spherical grains of TiO_2 are covered by cubic nano-crystals of MHCM. Furthermore, the composite materials show a red shift of the threshold absorption edge in the UV region, due to a decrease of the titanium dioxide band gap.

The waves of cyclic voltammetry and their dependence upon the K^+ concentration demonstrate the successful synthesis of both CoHCF and FeHCC [20,27]. Only a single quasi-reversible redox system is detected both in FeHCC and in CoHCF.

In bulk CoHCF, two redox processes due to the Fe^{III}/Fe^{II} and Co^{III}/Co^{II} couples, respectively, can be observed; the second one becomes electroactive only when the compound is crystallized in the so called "insoluble form"[51] or in nano-sized form[20]. In our bulk CoHCF, the peak potential and the E^0 values allow to assign the redox wave to Fe^{III}/Fe^{II} couple[20]. In the FeHCC compounds, the observed redox wave is still due the iron center, as confirmed by the E^0 values, while the cobalt center is non electroactive[27]. Hence the observed redox waves in TiO_2-FeHCC and TiO_2-CoHCF are always due just to the Fe^{III}/Fe^{II} couple.

From the CVs of TiO_2-FeHCC (Fig. 2 and Table 3) we obtain that, with increasing the TiO_2/FeHCC ratio, the kinetics of cation insertion becomes slower, since the cathodic peak shifts toward more negative potentials, while the kinetics of its release is faster, since the anodic peak shifts toward more negative potentials. Also the E° values show a negative shift in going from 1:1 to 10:1 composites, and no further changes in the 100:1 composite. The redox process is characterized by a relative high peak separation, in accordance with the published literature[27], while the peak shapes reflect the difference in the TiO_2-FeHCC synthesis. Actually, the modified electrode was realized by chemical synthesis (see experimental paragraph for details) while in the published literature[27], the TiO_2-FeHCC composite electrodes were electrochemically synthesized in situ on a TiO_2 thin film. In the case of TiO_2-CoHCF (Fig. 3 and Table 4), both cation insertion and release become more difficult at least for 1:1 and 10:1 compounds, while in 100:1 ratio the CV shape prevents the resolution of the voltammetric wave. In this case, as expected, the E° values remain constant.

Reaction Mechanism

IR, XPS and XAS and XANES results allow to tentatively identify possible reaction mechanisms for the formation of the composites. In the case of CoHCF and, more generally, in the case of metal hexacyanoferrates, the morphology of CN stretching band reflects the complexity of their structure. Actually, the possible co-presence of different linear chains, for example Fe^{III}-CN-Co^{II} or Fe^{II}-CN-Co^{III}, made possible by the redox properties of the two redox metal centers, leads to different chemical environments for the CN groups.[20] Further complexity can arise for the possible co-presence of the soluble and insoluble structure. On the other hand, in FeHCC the iron center is the only electroactive species; hence, the chemical differences in the chains are less than in the case of CoHCF.

The formation of MHCM cluster on the TiO_2 surface causes a clear modification of the IR spectra. The change in the intensity, that might be assigned to the different amounts of MHCM added and hence to the different degree of interaction with the TiO_2, is accompanied by a band shift towards lower wavenumbers and a shape morphology change (Fig. 7 and 8). IR results are in agreement with the XPS that allows to distinguish between Fe–CN (CoHCF) and Fe–NC (FeHCC) and confirm the absence of Fe^{III} in TiO_2-CoHCF samples with 1:1 (Fig. 9a) and 10:1 ratios (Supporting information Fig. S6) and the presence of Fe^{III} in the 100:1 sample (Supporting information Fig. S6). XPS and IR identification of cobalt species are also in agreement for both FeHCC and CoHCF samples. Furthermore XPS analyses provide the evidence of the interaction between nitrogen and titanium: cyanide groups may act as ligands for titanium ions at the surfaces, forming M–CN–Ti bonds, as also shown by the band shift towards lower wavenumbers and shape morphology change in IR spectra. The involved reaction might be thought as a nucleophilic substitution reaction with titanium ions playing the role of central ions and hexacyanoferrate anions acting as ligands.

The combined XANES and EXAFS analysis at the Ti K-edge of Fig. 13a and 13b show that the presence of MHCM modifies the local environment of the titanium, relative to that in pure anatase. This suggests the same type of binding between the anatase and either FeHCC or CoHCF cubes. The analysis at the metal (Fe and Co) K-edges shows modification in the XAS spectra respect to the pure CoHCF sample (and the same holds true for the FeHCC case of Fig. S11), thus confirming the occurrence of a close interaction between TiO_2 and CoHCF (or FeHCC). Overall, these findings are explained by considering a close interaction between the anatase and the FeHCC or CoHCF cubes, most likely through the N side of the CN moieties, as previously evidenced by the IR and XPS analyses.

On the basis of these findings two mechanisms for the metal hexacyanoferrate (FeHCC or CoHCF) interaction to the anatase particles can be proposed. According to the first mechanism, the HCC or HCF salt reacts with either Fe(III) or Co(III) respectively to give the mixed hexacyanometallate (I step, Fig. 14a) and subsequently the insoluble species, consisting in a dendrimer-like structure, reacts with the N terminals (II step, Fig. 14a). It is worth noting that the role of the vacancies is important because they suppress the perfectly cubic structure and increase the surface adhesion. The presence of ion vacancies, and their concentration, in metal hexacyanoferrates certainly affects a range of properties[52]. However, one may imagine another mechanism: the HCC or HCF salt reacts with anatase particles (I step, Fig. 14b) and, subsequently, the metal hexacyanometallate FeHCC or CoHCF synthesis occurs (II step, Fig. 14b). Presently, it is not possible to determine which of these two mechanisms is the predominant one.

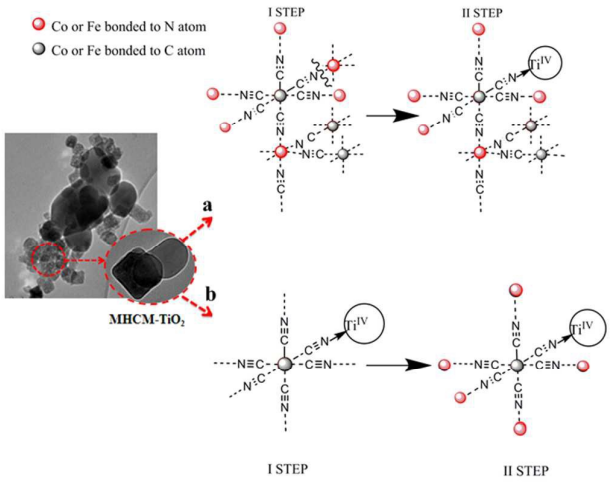

Fig. 14 Schematics of two possible mechanisms for the metal hexacyanometallate interaction with anatase particles. The red spheres are Co or Fe bonded to N atoms; the grey atoms are Co or Fe ions bonded to C atoms.

Modification of the TiO_2 optical properties

Since XPS provides the information on the total density of states of the valence band, changes in the valence band may reflect a modification of the optical properties of the composites compared to pure TiO_2. By comparing valence band spectra in pure TiO_2 and in the composites, we note changes of line-shape (Fig. 11,12) and a shift of the edge towards lower binding energies (Tables 6,7). According to previous DOS studies of doped TiO_2[53] the shift to lower energies determines the decrease in the band gap energy thus causing different optical properties for the composites compared to pure TiO_2.

In order to evaluate the effect of CoHCF or FeHCC doping upon TiO_2 absorption threshold, UV-Vis spectra were recorded in the 220–700 nm range in suspensions of TiO_2-CoHCF and TiO_2-FeHCC (Fig. 15,16). The progressive shift towards higher wavelengths of the TiO_2 absorption threshold is notable by adding $K_3[Fe(CN)_6]$ and $CoCl_2$ or $K_3[Co(CN)_6]$ and $FeCl_2$ with the formation of CoHCF or FeHCC, respectively, linked to the TiO_2. In both cases it is worth observing a shift of the threshold at lower energy that can be explained also on the basis of theoretical calculations[54]. In addition, new absorption bands in the UV and Vis region related to MHCMs play a fundamental role in the promotion of *titania* electrons to the conduction band with the same mechanism of TiO_2 dye solar cells. These findings are much relevant in all the applications of TiO_2 depending upon its light absorption capability.

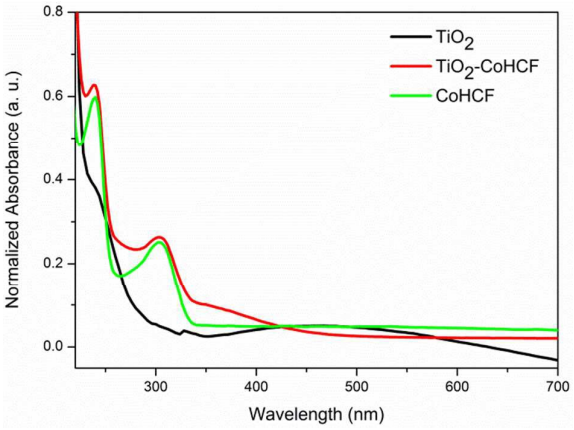

Fig. 15 UV-Vis spectra performed in a TiO_2-CoHCF suspension (10:1 ratio).

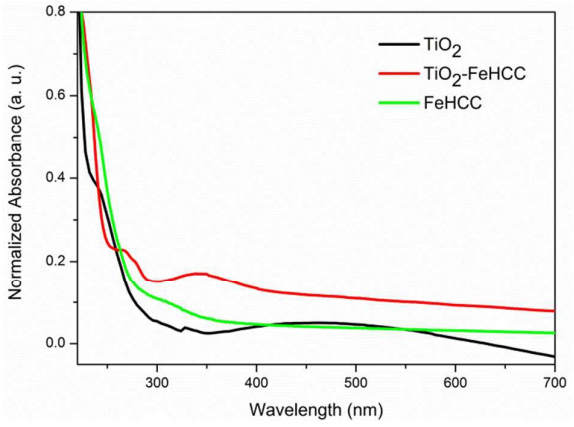

Fig. 16 UV-Vis spectra performed in a TiO_2-FeHCC suspension (10:1 ratio).

Evaluation of photocatalytic activity

TiO_2-CoHCF in 10:1 ratio compound has been directly used to evaluate its photocatalytic activity in photoelectrochemical degradation of methylene blue (MB) in aqueous solutions under UV irradiation. For comparison, native anatase TiO_2 was also tested.

MB has been chosen as a model to test the photocatalytic activity of surfaces in an aqueous medium in according with the International Standard ISO 10678.

The tests were performed by following the methodology reported in the previous cited ISO standard. The degradation reaction kinetics are studied by monitoring the variation of the normalized dye absorption spectra in function of the irradiation time with UV light in the wavelengths range between 220 and 750 nm, as shown in Fig. 17. In the case of TiO_2-CoHCF in 10:1 ratio, the decrease of the absorbance vs. time is faster than native TiO_2; the value of dA/dt for TiO_2-CoHCF is about 20% higher than the native TiO_2. The results revealed that the CoHCF doped TiO_2 showed higher photocatalytic activity than that of native TiO_2.

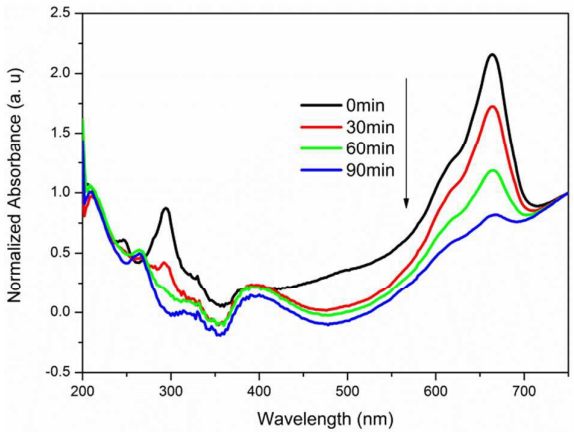

Fig. 17 CoHCF-TiO_2 1:10 UV-Vis spectra in the λ range between 220 and 750 nm.

Conclusions

New composite materials based on TiO_2-MCHM have been synthetized and characterized with a correlated use of many experimental techniques in order to assess the formation of MHCM compounds, to investigate its bonding to TiO_2 and, finally, to characterize the associated modifications of the optical properties of *titania*. In particular, the cyclic voltammetry and the morphological inspection by TEM, confirm the formation of CoHCF and FeHCC cubic crystals linked to TiO_2 particles in the composites. IR, XPS, and XAS suggest the formation of a well-defined bond between the nitrogen of the cyano-group and the titanium of the *titania* substrate. These findings suggest two possible mechanisms (Fig. 14) for the formation of MHCMs on *titania* surface. In the b mechanism in Fig. 14, the vacancy in the structures play a key role in the promotion of the N-Ti bond. This model is supported, in particular, by the evolution of the Co/Fe stoichiometric ratio going from the 1:1 to 100:1 in the TiO_2/CoHCF composites. Indeed, in the 1:1 compound, the Co/Fe ratio is 1, characteristic of the so called “soluble” form; with increasing the TiO_2 fraction, the Co/Fe region approaches the limit value of the so called ”insoluble” form, rich in vacancies of the $Fe(CN)_6^{3-}$ group. A similar trend occurs in the case of FeHCC. These observations make the b path more likely.

UV-Vis spectra and the valence band measurement in the composites confirm a desirable reduction of the TiO_2 band gap. The versatility of the synthesis permits to obtain both bulk and thin films composite materials. Practical use of these materials can be envisaged in different areas, such as antibacterial treatments, protection of historical artifacts, self-cleaning surfaces, photovoltaic cells.

Acknowledgements

XAS experiments at ELETTRA were supported by the proposal #20125309.

Sardinia Regional Government is gratefully acknowledged for the financial support (P.O.R. Sardegna F.S.E. Operational Program of the Regione Autonoma della Sardegna, European

Social Fund 2007 – 2013 – Axis IV Human Resources, Objective 1.3, Line of Activity 1.3.1 "Avviso di chiamata per il finanziamento di Assegni di Ricerca".

Electronic Supplementary Information (ESI) available free of charge via the Internet at http://pubs.acs.org.

1 A. Fujishima and K. Honda, *Nature,* 1972, **238**, 37.
2 Y. F. Zhu, J. Zhang, Y. Y. Zhang, M. Ding, H. Q. Qi, R. G. Du and C. J. Lin, *Acta Phys. Chim. Sin.,* 2012, **28**, 393.
3 G. Dai, L. Zhao, J. Li, L. Wan, F. Hu, Z. Xu, B. Dong, H. Lu, S. Wang and J. Yu, *J. Colloid Interface Sci.,* 2012, **365**, 46.
4 T. J. Ha, S. Y. Jung, J. H. Bae, H. L. Lee, H. W. Jang, S. J. Yoon, S. Shin, H. H. Cho and H. H. Park, *Microporous and Mesoporous Mater.,* 2011, **144**, 191.
5 D. Tahk, T. I. Kim, H. Yoon, M. Choi, K. Shin and K. Y. Suh, *Langmuir,* 2010, **26**, 2240.
6 F. R. Marciano, D. A. Lima-Oliveira, N. S. Da-Silva, A. V. Diniz, E. J. Corat and V. J. Trava-Airoldi, *J. Colloid Interface Sci.,* 2009, **340**, 87.
7 Graziani, L.; Quagliarini, E.; Osimani, A.; Aquilanti, L.; Clementi, F.; Yéprémian, C.; Lariccia, V.; Amoroso, S.; D'Orazio, M., *Build. Environ.*, 2013, **64**, 38.
8 M. C. Tsai, M. H. Yang, Y. W. Chang, J. K. Tzeng, C. Y. Lee, H. T. Chiu, H. C. Chen and I. N. Lin, *Mater. Chem. Phys*., 2013, **143**, 60.
9 Fujishima, A.; Zhang, X.; Tryk, D. A., *Surf. Sci. Rep.,* 2008, **63**, 515.
10 D. P. Serrano, G. Calleja, R. Sanz and P. Pizarro, *J. Mater. Chem.,* 2007, **17**, 1178.
11 I. A. Rutkowska, A. Andrearczyk, S. Zoladek, M. Goral, K. Darowicki and P. J. Kulesza, *J. Solid State Electrochem.,* 2011, **15**, 2545.
12 L. Guadagnini, D. Tonelli and M. Giorgetti, *Electrochim. Acta,* 2010, **55**, 5036.
13 M. Ciabocco, M. Berrettoni, S. Zamponi, J. A. Cox and S. Marini, *J. Solid State Electrochem*., 2013, **17**, 2445.
14 P. J. Kulesza, M. A. Malik, M. Berrettoni, M. Giorgetti, S. Zamponi, R. Schmidt and R. Marassi, *J. Phys. Chem. B,* 1998, **102**, 1870.
15 D. Iveković, H. V. Trbić, R. Peter, M. Petravić, M. Čeh and B. Pihlar, *Electrochim. Acta,* 2012, **78**, 452.
16 R. R. Sheha, *J. Colloid Interface Sci.,* 2012, **388**, 21.
17 I. Maurin, D. Chernyshov, F. Varret, A. Bleuzen, H. Tokoro, K. Hashimoto and S. Ohkoshi, *Phis. Rev. B,* 2009, **79**, 1.
18 R. A. Huggins, *J. Electrochem. Soc.,* 2013, **160**, 3020.
19 M. Giorgetti and M. Berrettoni, *Inorg. Chem*., 2008, **47**, 6001.
20 M. Berrettoni, M. Giorgetti, S. Zamponi, P. Conti, D. Ranganathan, A. Zanotto, M. L. Saladino and E. Caponetti, *J. Phys. Chem. C,* 2010, **114**, 6401.
21 M. Wilamowska and A. Lisowska-Oleksiak, *Solid State Ion.,* 2011, **188**, 118.
22 A. Widmann, H. Kahlert, I. Petrovic-Prelevic, H. Wulff, J. V. Yakhmi, N. Bagkar and F. Scholz, *Inorg. Chem.,* 2002, **41**, 5706.
23 M. Khoudiakov, A. L. Parise and B. S. Brunschwig, *J. Am. Chem. Soc.,* 2003, **125**, 4637.
24 N. R. de Tacconi, K. Rajeshwar and R. O. Lezna, *Electrochim. Acta,* 2000, **45**, 3403.
25 N. R. de Tacconi, J. Carmona and K. Rajeshwar, *J. Phys. Chem.,* 1997, **101**, 10151.
26 N. R. de Tacconi, K. Rajeshwar and R. O. Lezna, *J. Electroanal. Chem.,* 2001, **500**, 270.
27 M. Ciabocco, M. Berrettoni, D. F. Martino Chillura and M. Giorgetti, *Solid State Ion.,* 2014, **259**, 53.
28 T. J. B Holland and S. A. T. Redfern, *Mineral. Mag.,* 1997, **61**, 65.
29 M. P. Seah, *Surf. Interface Anal.,* 2001, **31**, 721.
30 N. Fairley, *CasaXPS*, version 2.3.15; 1999-2003.
31 D. A. Shirley, *Phys. Rev. B,* 1972, **5**, 4709.
32 M. P. Seah, *Quantification in AES and XPS*. In: Briggs D, Grant JT (eds) Surface Analysis by Auger and X-Ray Photoelectron Spectroscopy. IM Publication Surface Science Spectra, Manchester, 2003.
33 J. H. Scofield, *J. Electron. Spectrosc.,* 1976, **8**, 129.
34 R. F. Reilman, A. Msezane and S. T. J. Manson, *J. Electron. Spectrosc. Relat. Phenom.,* 1976, **8**, 389.
35 M. Fantauzzi, A. Pacella, J. Fournier, A. Gianfagna, G. B. Andreozzi and A. Rossi, *Anal. Bioanal. Chem*., 2012, **404**, 821.
36 M. P. Seah and W. A. Dench, *Surf. Interface Anal.*, 1979, **1**, 2.
37 B. Ravel and M. Newville, *J. Synchrotron Radiat.,* 2005, **12**, 537.
38 K. Oku, K. Wagatsuma and H. Matsuta, *J. Electron Spectrosc. Relat. Phenom.,* 1997, **83**, 31.
39 X. Cui, L. Hong and X. Lin, *J. Electroanal. Chem.,* 2002, **526**, 115.
40 M. Olla, G. Navarra, B. Elsener and A. Rossi, *Surf. Interface Anal.,* 2006, **38**, 964.
41 M. Fantauzzi, A. Pacella, D. Atzei, A. Gianfagna, G. B. Andreozzi and A. Rossi, *Anal. Bioanal. Chem.,* 2010, **396**, 2889.
42 D. Atzei, D. De Filippo, A. Rossi and R. Caminiti, *Spectrochim. Acta A,* 1993, **49**, 1779.
43 D. Atzei, D. De Filippo, A. Rossi, R. Caminiti and C. Sadun, *Spectrochim. Acta A*, 1995, **51**, 11.
44 D. Atzei, A. Rossi and C. Sadun, *Spectrochim. Acta A*, 2000, **56**, 1875.
45 H. Haraguchi, K. Jujiwara and K. Puwa, *Chem. Lett.,* 1975, 409.
46 T. R. I. Cataldi, G. E. De Benedetto and A. Bianchini, *Electroanal. Chem.,* 1998, **448**, 111.
47 W. Macyk, K. Szaciłowski, G. Stochel, M. Buchalska, J. Kuncewica and P. Łabuz, *Coord. Chem. Rev.,* 2010, **254**, 2687.
48 R. Sanjinés, H. Tang, H. Berger, F. Gozzo, G. Margaritondo and F. Lévy, *J. Appl. Phys.,* 1994, **75**, 2945.
49 K. Takegara and H. Harima, *Phase Transition*, 2002, **75**, 799.
50 M. Giorgetti, *ISRN Mater. Sci.,* 2013, **2013**, 1.
51 M. Berrettoni, M. Giorgetti, J. A. Cox, D. Ranganathan, P. Conti and S. Zamponi, *J. Solid State Electrochem*., 2012, **16**, 2861.
52 M. Giorgetti, L. Guadagnini, D. Tonelli, M. Minicucci and G. Aquilanti, *Phys. Chem. Chem. Phys.*, 2012, **14**, 5527.
53 T. Umebayashi, T. Yamaki, H. Itoh and K. Asai, *Appl. Phys. Lett.,* 2002, **81**, 454.
54 M. Berrettoni, T. Meneghelli, M. Giorgetti, R. Tarroni, E. Caponetti, M. L. Saladino, G. Nasullo, presented at the ISA 2010, Rimini, June, 2010.